

Satellite radar anisotropy observed in urban areas

Aaron C. Paget^{a*}, Steve Frolking^b, David G. Long^a, and Tom Milliman^b

^aBYU Center for Remote Sensing, Brigham Young University, Provo, UT, USA; ^bInstitute for the Study of Earth, Oceans, and Space, University of New Hampshire, Durham, NH, USA

(Received 20 August 2014; accepted 18 November 2014)

QuikSCAT backscatter is generally higher over urban areas than surrounding vegetated areas. Azimuthal anisotropy has been observed over some urban areas, but the strength of the azimuthal anisotropy in the urban backscatter signal has not been well quantified. This study investigates radar azimuthal anisotropy in urban areas. QuikSCAT L1B σ^0 observations are compared for urban, non-urban, and uninhabited regions to identify the magnitude and possible causes of anisotropic responses. The possible cause of azimuthal variations (AVs) in the data is the presence of corner reflectors, resulting from urban infrastructure and land use, including buildings, roads, and road structure. Backscatter characteristics for each urban area are shown to be closely related to road orientation and organization. Each region is found to have a unique backscatter signal and azimuthal response.

1. Introduction

Scatterometers, such as SeaWinds on QuikSCAT, rely on backscatter from the Earth's surface to determine surface characteristics of both land and water. Scatterometers emit an electromagnetic pulse that reflects and refracts off a surface. The portion of the signal that returns to the scatterometer is the backscattered signal. The strength of the normalized backscattered signal (σ^0 in dB) is a function of the surface characteristics. The surface roughness, reflectivity, and orientation relative to the incident beam affect σ^0 . QuikSCAT exploits these characteristics by using a rotating dish antenna that observes the surface from multiple azimuth angles (see Figure 1 in Spencer, Wu, and Long 2000). Observations from multiple azimuth angles are necessary to identify azimuthal variations (AVs) in σ^0 . Using AV in σ^0 , QuikSCAT retrieves vector winds over water (Liu 2002).

In addition to ocean wind vector studies, scatterometers have had numerous applications to terrestrial systems – for example, landscape freeze–thaw (Kimball et al. 2004; Bartsch et al. 2007), ice sheets (Ashcraft and Long 2006), soil moisture (Naeimi et al. 2009), vegetation canopy (Frolking et al. 2012; Long and Hardin 1994), and urban landscapes (Nghiem et al. 2009; Frolking et al. 2013).

Over land, Ku-band σ^0 varies with surface characteristics such as roughness, vegetation canopy density, dielectric properties, and presence of dihedral corner reflectors (Ulaby and Long 2014). As a result, QuikSCAT σ^0 will be sensitive to changes in built infrastructure density, as well as vegetation phenology, changes in vegetation cover, and other surface characteristics. A long-term metric of changes to these surface characteristics can provide valuable information for analysis of

*Corresponding author. Email: aaroncpaget@gmail.com

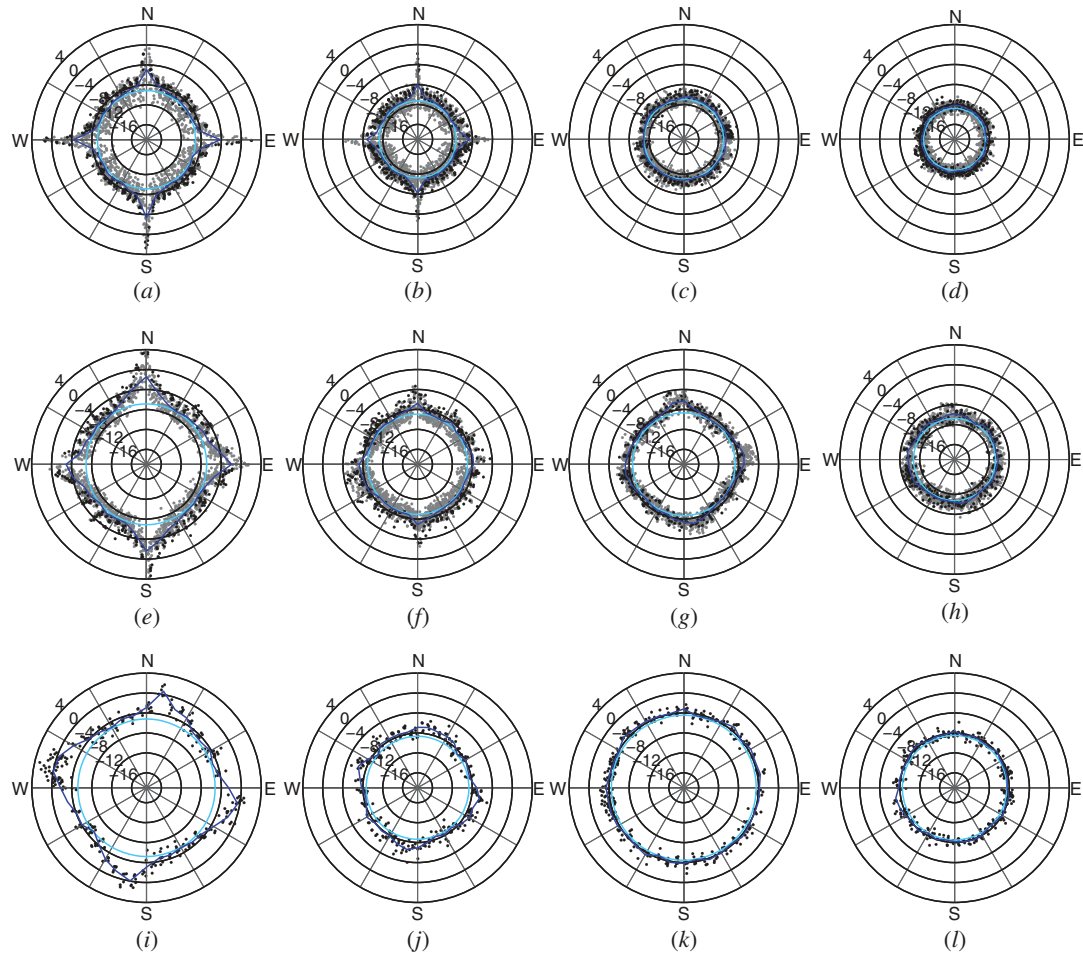


Figure 1. Magnitude and azimuthal angle for QuikSCAT L1B HH and VV σ^0 observations during 1 July 2003 through 31 August 2003 for (a) Phoenix – HH, (b) Phoenix – VV, (c) near-Phoenix – HH, (d) near-Phoenix – VV, (e) Beijing – HH, (f) Beijing – VV, (g) near-Beijing – HH, (h) near-Beijing – VV, (i) Mexico City – HH, (j) Mexico City – VV, (k) São Paulo – HH, and (l) São Paulo – VV. Black symbols specify observations from the smaller $0.2^\circ \times 0.2^\circ$ area; grey and black symbols together specify observations from the larger $0.5^\circ \times 0.5^\circ$ area. Directions relative to true north are indicated. Concentric circles indicate magnitude of σ^0 from 4 to -16 dB (outer ring to inner ring, respectively). The dark blue line represents the mean σ^0 in 10° bins; the light blue circle represents the σ^0 floor (average of mean σ^0 in the two lowest 10° bins).

geophysical processes that are naturally and anthropologically influenced. Such information can contribute to studies of interannual variability in vegetation phenology, surface colour, surface water dynamics, changes in land use, urbanization, and densification of urban areas; all these can have an impact on local and regional climate and extreme weather events (e.g. drought, flooding, urban heat islands). Our study of AV in σ^0 opens the door to further studies of these processes on the observed scatterometer signal in urban areas.

For native resolution (order of 20–30 km) scatterometer observations of land-based non-urban systems, AV has generally been assumed to be insignificant (e.g. Álvarez-Pérez, Marshall, and Gregson 2000). Nghiem et al. (2009) noted that this assumption is not valid for urban areas. After processing the QuikSCAT scatterometer L1B σ^0 data using a dense sampling technique to obtain subnative ($O(1$ km)) resolution for the data

by using long-term averaging (1 year), they found that dense and tall infrastructure were associated with increased values of σ^0 for six urban areas. The details regarding the effect of infrastructure on the azimuthal anisotropy of the retrieved backscatter signal were not specifically addressed. The possibility that anisotropy exists in the pre-processed data was also not evaluated. In this study, we assess the explicit azimuthal anisotropy in QuikSCAT scatterometer Level 1B native resolution (25 km) raw backscatter data from urban and non-urban landscapes. This is the first time we are aware of that anyone has analysed the raw data for azimuthal modulation over urban areas in this much detail.

The QuikSCAT scatterometer operates at a 2.8 cm wavelength with accuracy better than 0.1 dB (Wu et al. 2003; Kunz and Long 2005). QuikSCAT is a pencil beam scatterometer with a rotating dish and has vertical (VV) and horizontal (HH) polarizations with 54° and 46° incidence angles, respectively. It emits a microwave pulse and receives the backscatter from the reflected signal. Surface characteristics including absorption, scattering, beam relative orientation, and multi-path reflections affect the retrieved signal strength (Ulaby, Moore, and Fung 1981). Not all materials reflect equally; building materials and shapes affect the absorption and scattering. In particular, the orientation of a building or structure in relation to the scatterometer beam (or antenna) changes the amount of backscatter reflected from the building surface received by the antenna (Ulaby and Long 2014). Additionally, multiple scatter angles play a role with buildings and other structures. Buildings, curbs, and roads are examples of dihedral corner reflectors, which exhibit stronger σ^0 responses in specific directions. Surfaces normal to the incident beam also tend to produce increased backscatter as observed by the satellite.

On the scale of a scatterometer footprint (20–30 km), individual buildings or structures are not resolved, but the cumulative effect of multiple building scattering directed toward the sensor is observed in the scatterometer signal. A σ^0 baseline or floor is expected for a region (Nghiem et al. 2009), but corner reflectors enhance the backscatter over the baseline. The orientation of buildings and other infrastructure including curbs is often closely related to the orientation of roads in the region, particularly in denser urban areas. As a result, the orientation of roads is a reasonable proxy for the orientations of buildings and other infrastructure that can act as corner reflectors within the scatterometer footprint.

To identify some of the traits and causes of QuikSCAT AV, six different regions are selected each exhibiting different characteristics of land use, building types, and road structure and infrastructure. Data and methodology are discussed, followed by analyses of the observed σ^0 for the six representative regions. Additional regions are considered in Paget et al. (2014). Final conclusions and suggestions are made to exploit possible applications of the unique response of σ^0 .

2. Data and methodology

The data for this analysis comes from the QuikSCAT L1B 25 km data for both ascending and descending passes from 1 July 2003 through 31 August 2003. For this study, the raw eggs or cells are used instead of the wind vector cell composites, 12.5 km, slice, or ultra-high resolution. These other resolutions were analysed and have similar characteristics to the raw data here with varying amounts of increased noise and uncertainty. However, to ensure the characteristics and signals identified in this work do not result from processing techniques, only results using the raw data are

shown. Two consecutive months of data provide a sufficient sampling density to clearly identify AVs (Paget et al. 2014). Some limited angle ranges lack observations; however, the overall sampling density is sufficient for this analysis. A longer time series from June 2002 through November 2009 is also analysed to determine the influence of both seasonal variations and longer term urban growth on the σ^0 and AV signals. The cell centre position, σ^0 , and azimuthal angle of the satellite relative to north for each cell are used in the analysis. The magnitude of σ^0 is sensitive to surface characteristics including vegetation, infrastructure, and geological characteristics. HH and VV data are analysed independently. For this study, all data quality flags are required to be unset (indicating good data) to be included.

For six study regions – four urban and two non-urban – a $0.5^\circ \times 0.5^\circ$ and a $0.2^\circ \times 0.2^\circ$ box (only the latter for two of the regions) centred over the identified region are specified (Table 1). Care was taken to exclude large bodies of water from within each region as these would bias the land surface σ^0 results. Study regions were classified based on the percentage of 500 m pixels within the region classified as urban in the MODIS MDC12Q1 land-cover classification (Friedl et al. 2010). Regions are considered urban if >40% of 500 m pixels are classified as urban and urban core if >75% (Table 1). Mixed-use regions contain 5–10% 500 m urban pixels and rural regions <1% (Table 1). Rural areas contain no significant infrastructure. For urban areas, the latitude and longitude ranges were chosen to also minimize inclusion of adjacent agricultural areas, undeveloped land, and steep mountain slopes within the ranges. For non-urban areas, the ranges were chosen to minimize bodies of water and could allow smaller urban areas to be contained within the boxes.

The data are sampled for each study region by identifying and selecting all available and valid σ^0 observations from the dataset for the time period of interest with centre of the observation falling within the spatial range of each region (0.2° or 0.5° box). Observation centres must be contained within the region, but a cell measurement covers a $24 \text{ km} \times 31 \text{ km}$ ellipse for the inner beam and a $25 \text{ km} \times 35 \text{ km}$ for the outer beam (Spencer, Wu, and Long 2000), so observations can partially extend outside of the study region. The azimuthal angle of the satellite antenna relative to north for each observation and the σ^0 value associated with each observation are sampled for each cell.

Table 1. Region names with grid size, grid centre location, and number of valid QuikSCAT L1B σ^0 observations during July and August 2003.

Location	Latitude	Longitude	Grid size	% urban ^a	Category	Valid σ^0 observations
Phoenix	33.42°N	111.95°W	0.5°	48.2	Urban	1911
			0.2°	75.8	Urban core	301
Near-Phoenix	33.7°N	113°W	0.5°	0.2	Rural	1877
			0.2°	0.0	Rural	301
Beijing	39.92°N	116.42°E	0.5°	48.8	Urban	1922
			0.2°	98.3	Urban core	291
Near-Beijing	39.75°N	117.25°E	0.5°	5.4	Mixed land use	2004
			0.2°	10.2	Mixed land use	300
Mexico City	19.43°N	99.12°W	0.2°	96.4	Urban core	320
São Paulo	23.55°S	46.64°W	0.2°	99.0	Urban core	333

^aPercentage of MODIS 500 m pixels in region classified as urban in MCD12Q1 land-cover classification product for 2007 (Friedl et al. 2010).

Azimuthal anisotropy exists in several areas. To help identify the extent and strength of the anisotropy, the floor value, the peak height, the maximum binned mean difference (MBMD), and the modulation index are calculated for each region and polarization. The floor of the σ^0 values for each region and polarization is determined by separating the observations into 10° bins. The mean value of σ^0 for each bin is determined. The mean values from the two bins with the smallest mean σ^0 values are averaged. Bins without any observations are ignored. This new value is considered the floor for this study. The peak value is established as the value of the 99th percentile of all observations, regardless of the angle. The peak height is the difference of the peak value and the floor value. The MBMD is the difference between the maximum and minimum 10° azimuth bin means. Any MBMD values >1.5 dB are typically associated with AV.

AV has been previously studied in the Polar Regions, and simple modulation models and indexes are developed (Long and Drinkwater 2000; Ashcraft and Long 2006). The modulation index used in this study is defined as follows. The index is the difference between the monthly means of the σ^0 observations in dB for two directions. The means are calculated from the observations within a 30° azimuth window centred on the maximum value and from a 30° window centred 45° clockwise from the maximum value; azimuth bins are fixed in this analysis. A trailing 12-month rectangular mean filter is applied to the monthly modulation indices for a given region to get the reported monthly modulation. Because the angles are fixed, regions with minimal azimuthal anisotropy can produce a negative value for the modulation index, while regions with significant azimuthal anisotropy produce positive values.

The regional azimuthal response of σ^0 is divided into three classes: (1) σ^0 is strong function of the azimuth angle (φ) and forms catenary shapes in a polar plot, (2) σ^0 is a weak function of φ and forms square shapes or slight catenary shapes (weak peaks) in a polar plot, or (3) σ^0 is not a function of φ and forms a circular shape in a polar plot (σ^0 is isotropic with φ). The azimuthal response of σ^0 was analysed for many locations in the analysis (Paget et al. 2014), but only four representative cities (Beijing, China; Phoenix, Arizona; Mexico City, Mexico; and São Paulo, Brazil) and two neighbouring areas (near-Beijing, China and near-Phoenix, Arizona) are reported here as examples of the characteristics of AV and radar anisotropy. The monthly mean is calculated for 30° azimuthal bins of the data. For the longer time series, the monthly mean is calculated for the same bins as well as a monthly mean across all azimuth angles. AV and radar anisotropy as well as seasonal and longer term changes are observed from Hovmöller diagrams of the time series of the data.

3. Observations

While each of the urban areas analysed have been built and expanded over one to many centuries, different zoning or building guides and laws have dictated the form and material of much of the construction of the urban areas. The resulting distribution appears to affect the backscatter measured by scatterometers and its azimuthal dependence. Four cities and two neighbouring non-urban areas identify AV in σ^0 caused by the dominant orientation of the city roads, the type of structures in the area, and the absence of urban development.

3.1. Raw observations

The Phoenix region contains one of the most consistent large-scale regular grid road systems in the USA, having grown from early settlements in the Salt River Valley (Jones

1890) using a planned regular grid system (Parera 2005). The primary roadways running through the region are oriented north–south and east–west. This orientation is consistent through the majority of the secondary and local roads. The buildings are dominantly individual homes spaced apart with some vegetation in between. The azimuthal response for Phoenix indicates σ^0 as a strong function of φ for the 2-month period of July and August of 2003 (Figures 1(a) and (b)). Peaks in σ^0 can be seen at the cardinal directions, consistent with the antenna being normal to building walls that are oriented with cardinal directions. For HH, the σ^0 floor values are about -9.15 dB with the peaks at 9.33 dB above the floor (Table 2). For VV, the σ^0 floor values are about -11.28 dB with the peaks at 5.98 dB above the floor, but the width of the angle for the increased response is narrower for VV. The MBMD is 5.8 and 3.3 dB for HH and VV, respectively (Table 2), because of the peaks in the noted azimuth directions.

Near-Phoenix, an unpopulated desert area with virtually no urban infrastructure, σ^0 is approximately isotropic with floors of -11.01 and -12.79 dB for HH and VV, respectively (Figures 1(c) and (d)). The MBMD is 0.65 and 0.69 dB for HH and VV, respectively (Table 2). The main difference between the Phoenix and near-Phoenix regions is the urban infrastructure. The floor value in Phoenix is elevated over the near-Phoenix region by 1.86 and 1.51 dB for HH and VV, respectively, but the Phoenix region also shows the catenary-like response in σ^0 with φ , while near-Phoenix does not.

The Beijing region has a gridded road structure dating back centuries (K. Seto, personal communication, 2013). The road structure is oriented north–south and east–west, like Phoenix, but the infrastructure includes large buildings and apartment complexes with little green space, though some variations do exist, especially outside of the main city. The buildings are densely packed in the city. Beijing shows peaks in

Table 2. Regional QuikSCAT L1B σ^0 characteristics for July–August 2003 (floor, peak height, MDMB) or June 2002 to November 2009 (modulation index and σ^0 trend). MBMD is the maximum binned mean difference as defined in Section 2.

HH					
Location	σ^0 Floor (dB)	σ^0 Peak Ht. (dB)	MBMD (dB)	Modulation Index (dB)	σ^0 trend 1999–2009 (dB year ⁻¹)
Phoenix	-9.15	9.33	5.82	2.6	0.087
Near-Phoenix	-11.01	2.06	0.65	0.4	0.002
Beijing	-6.88	8.25	5.47	3.6	0.37
Near-Beijing	-8.69	3.71	2.46	1.7	0.182
Mexico City	-5.21	7.19	5.95	4.1	0.086
São Paulo	-4.45	2.25	1.33	0.4	0.087
VV					
Location	σ^0 Floor (dB)	σ^0 Peak Ht. (dB)	MBMD (dB)	Modulation Index (dB)	σ^0 trend 1999–2009 (dB year ⁻¹)
Phoenix	-11.28	5.98	3.30	1.4	0.087
Near-Phoenix	-12.79	1.99	0.69	0.4	-0.003
Beijing	-8.95	4.28	2.20	1.2	0.392
Near-Beijing	-10.76	2.49	1.37	0.9	0.179
Mexico City	-8.67	3.85	2.36	1.3	0.1
São Paulo	8.5	2.36	1.50	0.6	0.113

σ^0 at the cardinal directions, like Phoenix, but the floor is -6.88 dB with peaks about 8.25 dB above the floor for HH and a floor of -8.95 dB with peaks 4.28 dB above the floor for VV (Figures 1(e) and (f)). The MBMD is 5.47 and 2.20 dB for HH and VV, respectively (Table 2). Compared with Phoenix, the overall mean difference for the period of July and August 2003 for Beijing is 3.9 dB for HH, indicating that Beijing is more reflective than Phoenix. The main peaks appear slightly broader than the peaks for Phoenix for both polarizations, and the overall signal strength is much larger in Beijing than Phoenix.

The region near-Beijing contains over 1000 small communities separated by cropland (as identified by visual inspection from Google Earth imagery). The communities generally have a regular gridded road system with an orientation rotated between 5° and 10° counterclockwise of the cardinal directions. The orientation of the small towns is evident in the shape of the azimuthal response of σ^0 (Figure 1(g)) even though the individual communities are much smaller than QuikSCAT's native resolution. Unlike the Beijing region, the peaks in σ^0 are weaker, consistent with infrastructure being generally oriented over the region but not strictly oriented like in Beijing. The strength of σ^0 is azimuth dependent. For HH, the peaks are only 3.71 dB over the -8.69 dB floor, but for VV, the signal is nearly isotropic at -10.76 dB with very weak peaks (Figure 1(h)). The MBMD is 2.46 and 1.37 dB for HH and VV, respectively (Table 2). The region has a floor response of ~ 2 dB smaller than the floor for Beijing.

Mexico City's major road network is oriented roughly 12° east of the cardinal directions, but the roads and structures are not consistently aligned over the entire region. In this region, backscatter peaks vary 4° – 5° in either direction of the main orientation. Mexico City covers a smaller area and only has a $0.2^\circ \times 0.2^\circ$ area for this study (to avoid high mountains to the north, west, and south, and a large lake to the east), resulting in fewer observations than the larger areas previously analysed (Table 1) and higher frequency sampling of the urban core. For HH, the σ^0 floor is -5.21 dB with peaks extending 7.19 dB above the floor, and for VV, the peaks extend 3.85 dB above the -8.67 dB base (Figures 1(i) and (j)). The azimuthal response dependence on φ is similar to the near-Beijing region, but the signal strength is much larger. The MBMD is 5.95 and 2.36 dB for HH and VV, respectively (Table 2), the largest of the six regions in this article. The buildings in Mexico City are densely packed with a wide variety of building types. The orientation of the roads is consistent with the orientation of the peaks in σ^0 , indicating that road and building orientations are important in identifying azimuthal anisotropy.

In comparison to Mexico City, the urban infrastructure of São Paulo is similarly dense and covers a similar area, but the road system is not consistently oriented. As a result, the σ^0 floor is -4.45 and -8.50 dB for HH and VV, respectively, and is isotropic with φ (Figures 1(k) and (l)). The MBMD is 1.33 and 1.50 dB for HH and VV, respectively (Table 2). No azimuthal peaks are evident in the σ^0 signal, but the overall signal strength is as high as any of the other cities analysed.

3.2. Seasonal observations

The general characteristics noted for each region for the 2-month period analysed exist throughout the entire dataset; however, the signal can change seasonally and over time. The monthly binned mean values for Phoenix from June 2002 through November 2009 show the same azimuthal peak pattern (Figures 2(a) and (b)), but additional variation exists on a subannual basis consistent with local seasons,

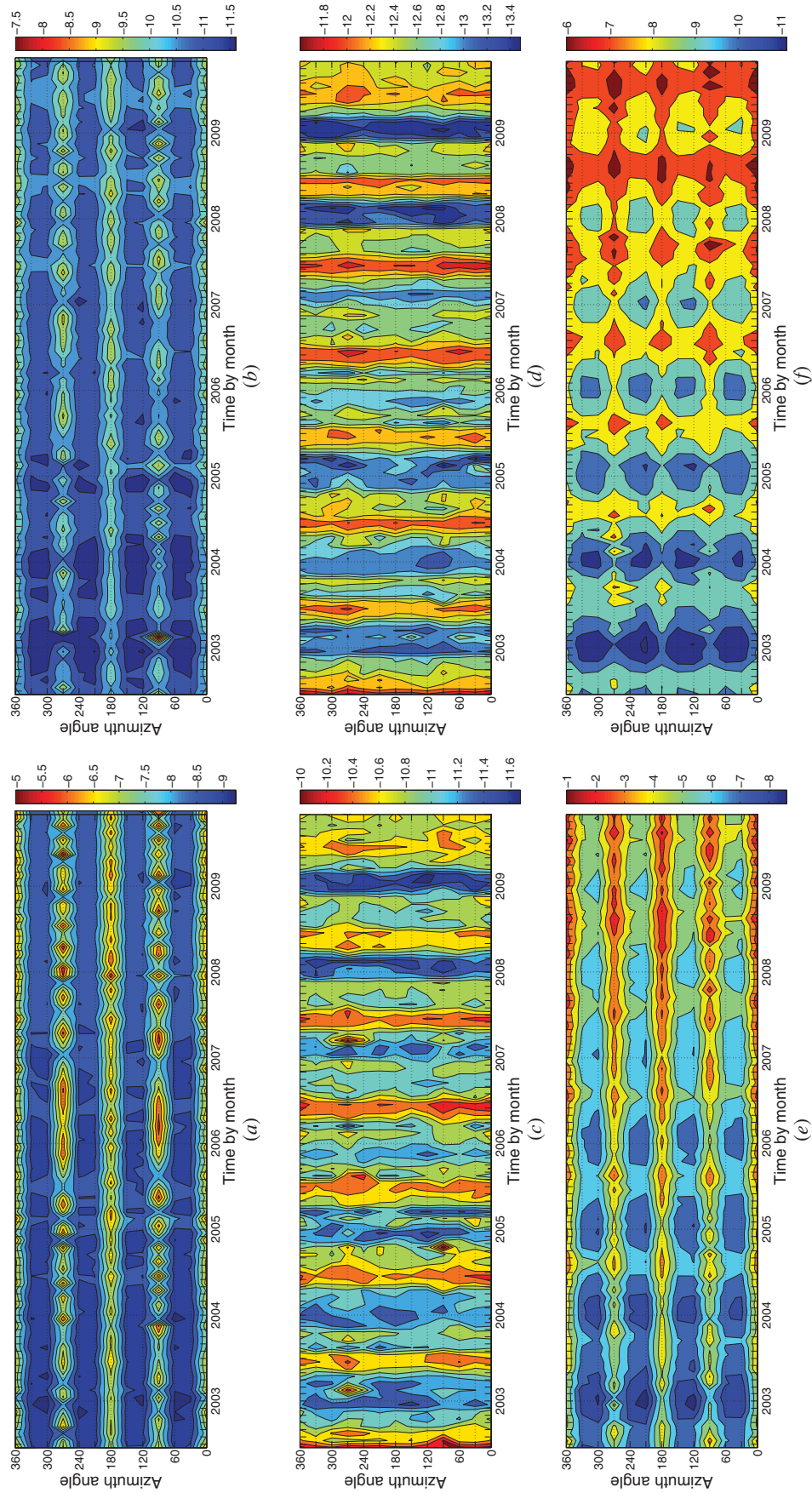


Figure 2. Hovmöller diagrams of the time series of the monthly mean (abscissa) of the 30° binned (ordinate) QuikSCAT LIB σ^0 data (in dB) across the boxes for (a) Phoenix ($0.5^\circ \times 0.5^\circ$) – HH, (b) Phoenix ($0.5^\circ \times 0.5^\circ$) – VV, (c) Phoenix ($0.5^\circ \times 0.5^\circ$) – HH, (d) Phoenix ($0.5^\circ \times 0.5^\circ$) – VV, (e) Phoenix ($0.5^\circ \times 0.5^\circ$) – HH, (f) Phoenix ($0.5^\circ \times 0.5^\circ$) – VV, (g) Phoenix ($0.5^\circ \times 0.5^\circ$) – HH, (h) Phoenix ($0.5^\circ \times 0.5^\circ$) – VV, (i) Phoenix ($0.5^\circ \times 0.5^\circ$) – HH, (j) Phoenix ($0.5^\circ \times 0.5^\circ$) – VV, (k) Phoenix ($0.2^\circ \times 0.2^\circ$) – HH, and (l) Phoenix ($0.2^\circ \times 0.2^\circ$) – VV.

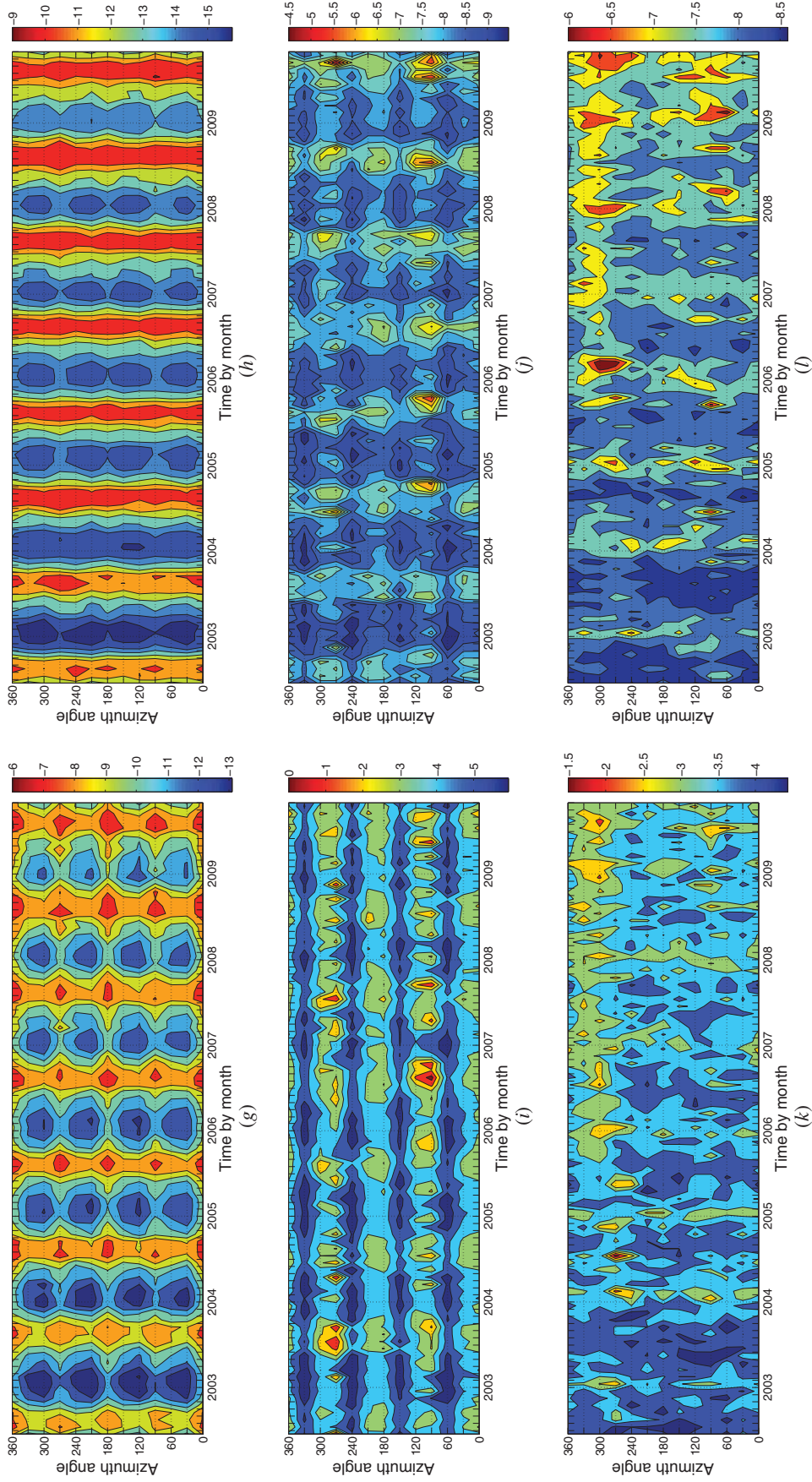


Figure 2. (Continued).

including precipitation and vegetation (Friesen, Steele-Dunne, and van de Giesen 2012; Steele-Dunne, Friesen, and van de Giesen 2012), though urban vegetation may be irrigated during the dry season, reducing its seasonality. A long-term increase in the signal also exists with an annual mean increase of 0.087 and 0.087 dB year⁻¹ for HH and VV, respectively (Figure 3(a)), consistent with increasing urban densification of infrastructure.

The neighbouring region, near-Phoenix, shows strong seasonal variation in backscatter across all azimuth angles, consistent with the natural seasonality of precipitation and vegetation (Figures 2(c) and (d)). The seasonal variations are the dominant signal. Long-term changes in the signal are negligible and well within the margin of error, with 0.002 and -0.003 dB year⁻¹ for HH and VV, respectively (Figure 3(b)), consistent with no trends in the surface characteristics.

For Beijing, seasonal variations exist and are of similar magnitude, 2–3 dB, to the AVs (Figures 2(e) and (f)). The seasonal changes in the signal are consistent with the local growing seasons where signal increases with vegetation foliage and water content. Long-term changes in the signal are significant with an annual mean increase of 0.370 and 0.392 dB year⁻¹ for HH and VV, respectively (Figure 3(c)). The long-term increase is consistent with increasing urban densification of infrastructure. The orientation of the peaks does not change over time, and the seasonal cycle slightly weakens with time. If we assume that vegetation is the dominant source for the seasonal cycle, then we can speculate that long-term growth can have the effect of removing vegetation or blocking vegetation from the field of view (possibly by making buildings taller or space between buildings narrower). For Beijing and other regions, a combination of these principles is the likely cause of the decrease in the seasonal variations. Additional analysis would require information regarding changes in infrastructure, densification of buildings, land-use changes, and vegetation growth.

Near-Beijing, a mixed-use agricultural area with small urban locations, variations in the seasonal signal is larger than the AVs, particularly for VV polarization (Figures 2(g) and (h)). The frequency of the seasonal changes is similar to those in Beijing, but the signal change is much larger, consistent with increased area covered by vegetation. Long-term changes in the signal exist with an annual mean increase of 0.182 and 0.179 dB year⁻¹ for HH and VV, respectively (Figure 3(d)), consistent with increasing urban densification of infrastructure or urban infrastructure replacing agricultural area. Changes in precipitation, irrigation, crop choice, and harvest timing may also affect the seasonal signal.

For Mexico City, seasonal variations, though smaller than the AVs, are clear in the signal (Figures 2(i) and 2(j)). The seasonal changes are consistent with increased vegetation during summer months. Long-term changes in the signal exist with an annual mean increase of 0.086 and 0.100 dB year⁻¹ for HH and VV, respectively (Figure 3(e)), consistent with increasing urban densification of infrastructure. New urban structure that does not maintain the same orientation as the overall area will strengthen the floor of the signal, not necessarily the signal in the direction of the known peaks.

São Paulo does not have the same AVs as Mexico City, though seasonal variations exist (Figures 2(k) and (l)). The seasonal variations are weaker than Mexico City, consistent with less vegetation, and the peak seasonal variations are offset, consistent with the local summer when vegetation grows. Long-term changes in the signal are similar to Mexico City with an annual mean increase of 0.087 and 0.113 dB year⁻¹ for HH and VV, respectively (Figure 3(f)), consistent with increasing urban densification of infrastructure.

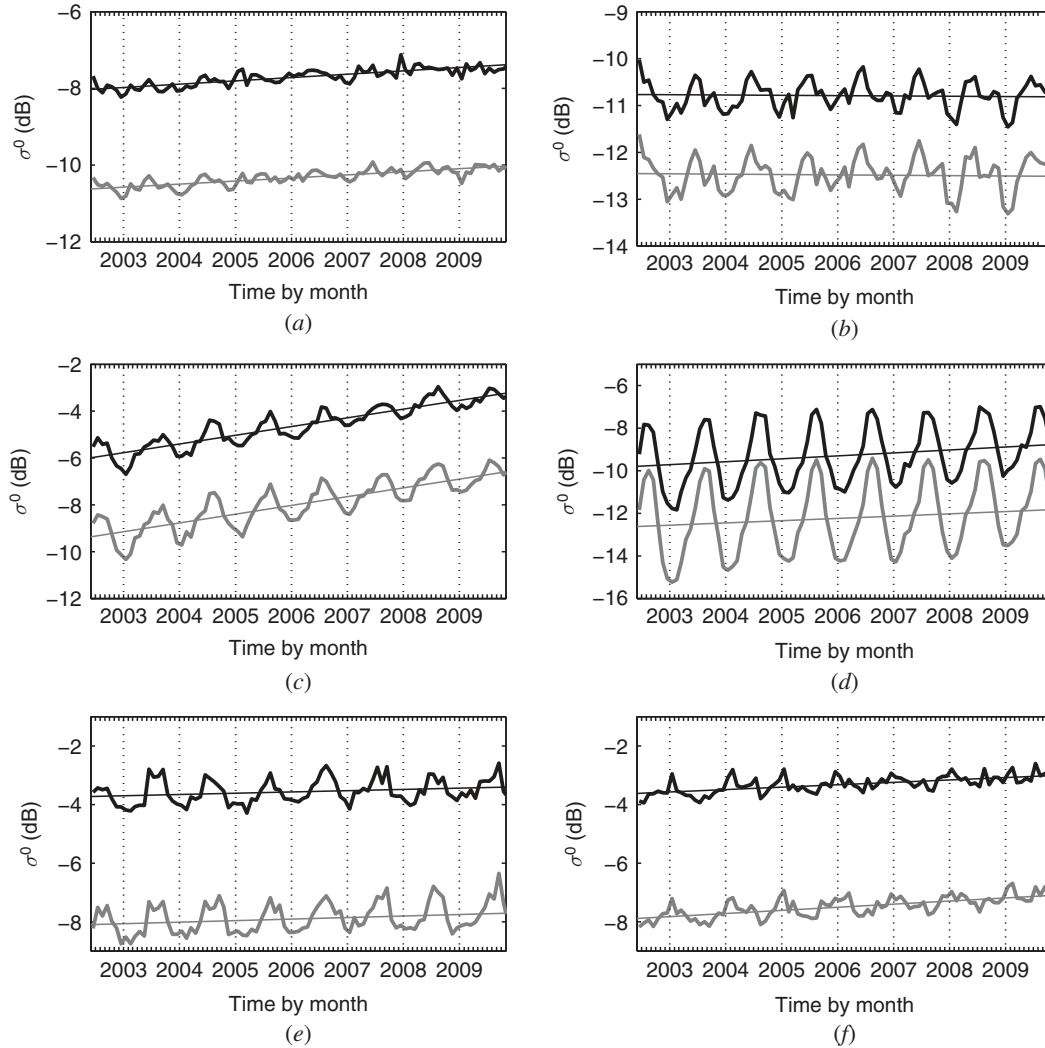


Figure 3. Monthly mean of the QuikSCAT L1B σ^0 data (thick line) and the linear fit (thin line) across the boxes for HH (black) and VV (grey) for (a) Phoenix ($0.5^\circ \times 0.5^\circ$), (b) near-Phoenix ($0.5^\circ \times 0.5^\circ$), (c) Beijing ($0.5^\circ \times 0.5^\circ$), (d) near-Beijing ($0.5^\circ \times 0.5^\circ$), (e) Mexico City ($0.2^\circ \times 0.2^\circ$), and (f) São Paulo ($0.2^\circ \times 0.2^\circ$). There were O(1000) valid σ^0 data points for each month in each $0.5^\circ \times 0.5^\circ$ box and O(150) for each $0.2^\circ \times 0.2^\circ$ box.

The modulation index of the signal for each of the regions exhibiting AVs is nearly constant for both polarizations from 2002 to 2009 and approximately zero for the isotropic regions (Figure 4). The consistent modulation index aids in identifying the seasonal and long-term changes in the mean signal. The region near-Beijing, for example, shows a long-term increase in σ^0 along with seasonal variations on a sub-year time scale with the amplitude of the signal related to seasonal effects. The amplitude of the seasonal signal decreases with increasing long-term mean, likely caused by an increase in infrastructure and decrease in agriculture. Similar decreases in the amplitude of the seasonal signal are present to a lesser extent in other urban areas, indicating an increasing densification of urban infrastructure and a decrease in vegetation cover as observed from the sensor.

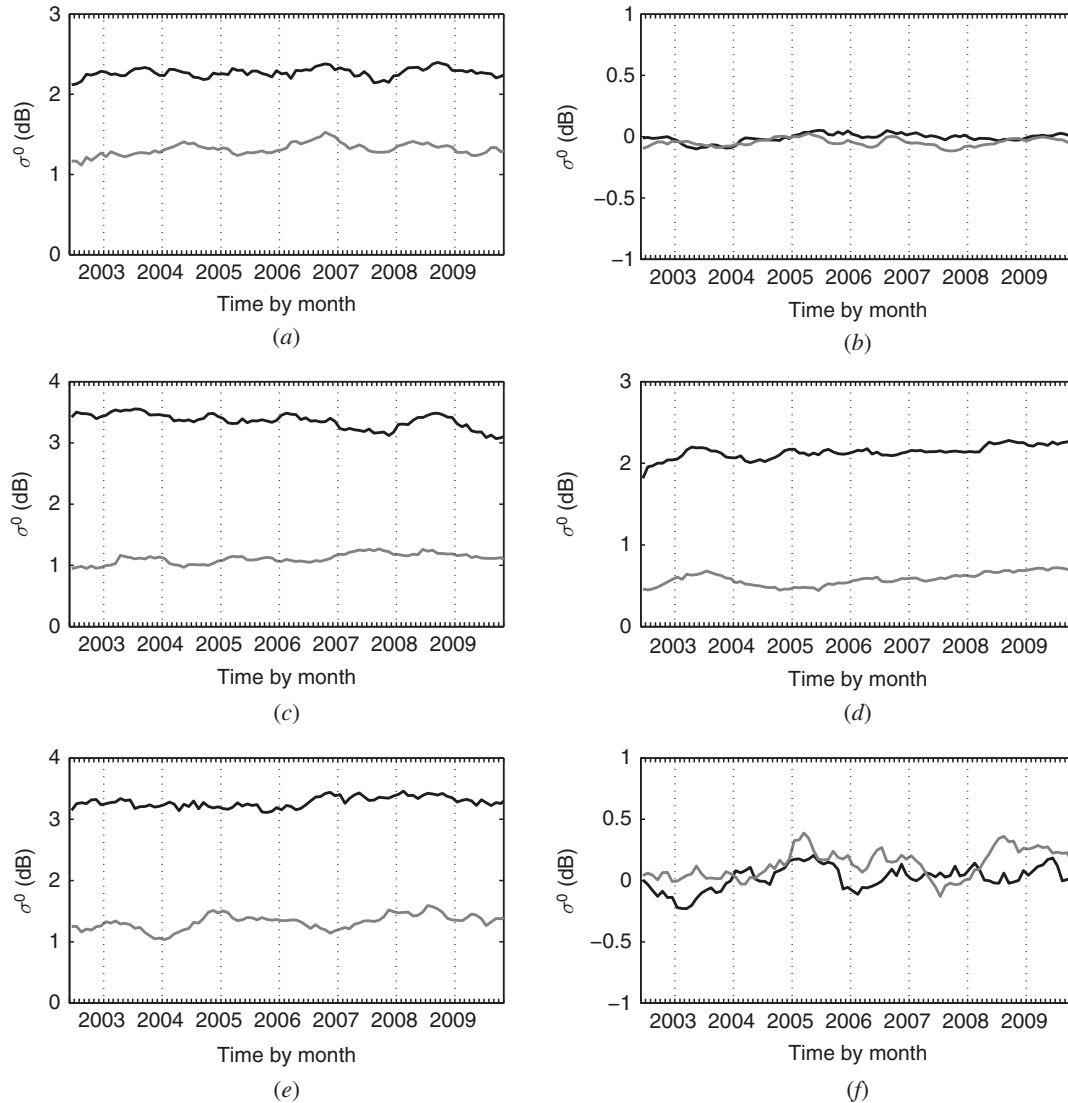


Figure 4. Modulation index of the QuikSCAT L1B σ^0 data as described in Section II for HH (black) and VV (grey) for (a) Phoenix ($0.5^\circ \times 0.5^\circ$), (b) near-Phoenix ($0.5^\circ \times 0.5^\circ$), (c) Beijing ($0.5^\circ \times 0.5^\circ$), (d) near-Beijing ($0.5^\circ \times 0.5^\circ$), (e) Mexico City ($0.2^\circ \times 0.2^\circ$), and (f) São Paulo ($0.2^\circ \times 0.2^\circ$).

4. Discussion

After careful analysis of the data for over 23 locations globally (Paget et al. 2014) with characteristics from the three classes, six are presented to illustrate characteristics which suggest that an anthropogenic source of AVs in the backscatter signal, σ^0 , occurs in urban areas with highly organized street systems. The variations occur in the horizontal polarization and, to a lesser extent in some urban areas, the vertical polarization, but not all urban areas show AV. The urban areas with a consistent gridded road system show AV elevated above the AV of urban areas without gridded road systems, and significantly above the AV of similar regions lacking urban infrastructure. The urban centres show increased σ^0 values over 2002–2009, consistent with increased building density (Frolking et al. 2013). However, the AV modulation index, which quantifies the magnitude of difference between peak and floor backscatter strength across azimuth, does not show a

significant trend during 2002–2009 for any of the regions (Figure 4). This indicates that urban development patterns followed the basic road orientation pattern that is present in 2003 in all cases.

In addition to the AV found in multiple regions with urban development, the number of available σ^0 observations for each region is directly proportional to the size of the region. Increasing the size of the region is only appropriate if the larger region is consistent in land cover with the smaller region. For both Beijing and Phoenix, the backscatter floor was 2–3 dB lower outside the 0.2° urban core region (Figures 1(a), (b), (e), and (f)). With a 4-day repeat orbit and a rotating pencil beam antenna, several orbits are required to compile observations at all angles; 16 days of observations ensures adequate sampling to identify dependence of σ^0 on φ for the study regions. We note that the length of the time period needs to be carefully considered since seasonal changes in the magnitude of σ^0 can exceed the size of the variations with AV.

Seasonal changes are present in σ^0 at all sites, though more pronounced for the two non-urban sites than for the four urban/urban core sites (Figure 2); vegetation phenological dynamics are likely the principal contributor to the seasonal signal variations, but a definite conclusion is beyond the scope of this article. Other potential contributions include precipitation and vegetation type. These potential contributors as well as land-use change might also affect the long-term changes. Anthropogenic influences, including changes urban infrastructure, contribute to long-term changes and change the surface reflectivity properties in the regions studied. The long-term changes were identified with a simple linear fit to the data; however, the actual effects of urban changes are not necessarily linear. The combination of the seasonal and long-term changes has potential to identify urban growth and densification on a regional basis, though a specific metric for this type of analysis is left for future studies. Information on vegetation, urban growth and densification, land-use changes, and soil moisture would aid in identifying and defining variation in the backscatter signal.

5. Conclusions

Azimuthal anisotropy in urban and non-urban regions can be directly linked to infrastructure, but we find different responses for different cities depending on the level of organization of the roads, buildings, and other infrastructure. For cities with highly organized road systems, the dominant direction of the roads indicates the angles where σ^0 is magnified significantly above a floor level. Backscatter AV for regions without consistent road systems is more isotropic. Infrastructure density and the magnitude of AV both appear to affect the strength of the σ^0 floor for the region. Long-term signal growth is linked to densification of urban infrastructure; AV does not have a long-term trend in urban or non-urban sites. Both σ^0 and backscatter AV modulation index values are higher for HH polarization than for VV polarization.

Additional considerations outside of the immediate scope of this article could also include types and sizes of buildings, building material, land use, building density, characteristics of the roads and curbs, vegetation, soil type and moisture, and precipitation. Some of these factors exhibits short-term variation (e.g. precipitation and soil moisture), annual phenology (e.g. vegetation canopies), relatively abrupt step changes (e.g. built infrastructure construction or demolition), and/or some long-term trends (e.g. building and road density). The reflective properties and influence of these parameters on the observed σ^0 are not explored here, but merit further investigation in the future to accurately understand their effects on σ^0 . Buildings and other infrastructure change with

growth and development. Changes to the built infrastructure including urbanization and changes in building material and land use will also influence observed σ^0 (Frolking et al. 2013), but the effects of these changes is likely unique to each region since regions change at different rates.

It is evident that AV exists within σ^0 observations of urban landscapes. The presence of dihedral corner reflectors such as buildings and curbs increases the backscatter signal. The consistent organization of these dihedral corner reflectors over large areas (O(cell size)) increases the azimuthal anisotropy of the system in urban and non-urban areas where anthropogenic influences are present. The applications of these findings can extend to many fields. Immediate future work includes analysis of seasonal changes, comparison with vegetation index, precipitation, urban changes over the lifetime of QuikSCAT, additional scatterometers (Oceansat-2 and ASCAT) and resolutions including slice data and ultra-high resolution (Ulaby and Long 2014).

Acknowledgement

We thank the anonymous reviews for comments on an earlier draft that improved the article.

Disclosure statement

No potential conflict of interest was reported by the authors.

Funding

This study was partially supported by NASA grants [NNX08AE59G, NNX10AP11G, NNX14AI70G].

References

- Álvarez-Pérez, J. L., S. J. Marshall, and K. Gregson. 2000. "Resolution Improvement of ERS Scatterometer Data over Land by Wiener Filtering." *Remote Sensing of Environment* 71 (3): 261–271. doi:10.1016/S0034-4257(99)00071-1.
- Ashcraft, I. S., and D. G. Long. 2006. "Relating Microwave Backscatter Azimuth Modulation to Surface Properties of the Greenland Ice Sheet." *Journal of Glaciology* 52 (177): 257–266. doi:10.3189/172756506781828764.
- Bartsch, A., R. Kidd, W. Wagner, and Z. Bartalis. 2007. "Temporal and Spatial Variability of the Beginning and End of Daily Spring Freeze/Thaw Cycles Derived from Scatterometer Data." *Remote Sensing of Environment* 106: 360–374. doi:10.1016/j.rse.2006.09.004.
- Friedl, M. A., D. Sulla-Menashe, B. Tan, A. Schneider, N. Ramankutty, A. Sibley, and X. M. Huang. 2010. "MODIS Collection 5 Global Land Cover: Algorithm Refinements and Characterization of New Datasets." *Remote Sensing of Environment* 114 (1): 168–182. doi:10.1016/j.rse.2009.08.016.
- Friesen, J., S. C. Steele-Dunne, and N. van de Giesen. 2012. "Diurnal Differences in Global ERS Scatterometer Backscatter Observations of the Land Surface." *IEEE Transactions on Geoscience and Remote Sensing* 50 (7): 2595–2602. doi:10.1109/TGRS.2012.2193889.
- Frolking, S., S. Hagen, T. Milliman, M. Palace, J. Z. Shimbo, and M. Fahnestock. 2012. "Detection of Large-Scale Forest Canopy Change in Pan-Tropical Humid Forests 2000–2009 with the SeaWinds Ku-Band Scatterometer." *IEEE Transactions on Geoscience and Remote Sensing* 50: 2603–2617. doi:10.1109/TGRS.2011.2182516.
- Frolking, S., T. Milliman, K. C. Seto, and M. A. Friedl. 2013. "A Global Fingerprint of Macro-Scale Changes in Urban Structure from 1999 to 2009." *Environmental Research Letters* 8: 024004. doi:10.1088/1748-9326/8/2/024004.

- Jones, D. W. 1890. *Forty Years among the Indians: A True yet Thrilling Narrative of the Author's Experiences among the Natives*. Salt Lake City, UT: Juvenile Instructor Office.
- Kimball, J. S., K. C. McDonald, S. Frolking, and S. W. Running. 2004. "Radar Remote Sensing of the Spring Thaw Transition across a Boreal Landscape." *Remote Sensing of Environment* 89: 163–175. doi:10.1016/j.rse.2002.06.004.
- Kunz, L. B., and D. G. Long. 2005. "Calibrating SeaWinds and QuikSCAT Scatterometers Using Natural Land Targets." *IEEE Geoscience and Remote Sensing Letters* 2 (2): 182–186. doi:10.1109/LGRS.2004.842468.
- Liu, W. T. 2002. "Progress in Scatterometer Application." *Journal of Oceanography* 58: 121–136. doi:10.1023/A:1015832919110.
- Long, D. G., and M. R. Drinkwater. 2000. "Azimuth Variation in Microwave Scatterometer and Radiometer Data Over Antarctica." *IEEE Transactions on Geoscience and Remote Sensing* 38 (4): 1857–1870. doi:10.1109/36.851769.
- Long, D. G., and P. Hardin. 1994. "Vegetation Studies of the Amazon Basin Using Enhanced Resolution Seasat Scatterometer Data." *IEEE Transactions on Geoscience and Remote Sensing* 32 (2): 449–460. doi:10.1109/36.295059.
- Naeimi, V., K. Scipal, Z. Bartalis, S. Hasenauer, and W. Wagner. 2009. "An Improved Soil Moisture Retrieval Algorithm for ERS and METOP Scatterometer Observations." *IEEE Transactions on Geoscience and Remote Sensing* 47 (7): 1999–2013. doi:10.1109/TGRS.2008.2011617.
- Nghiem, S. V., D. Balk, E. Rodriguez, G. Neumann, A. Sorichetta, C. Small, and C. D. Elvidge. 2009. "Observations of Urban and Suburban Environments with Global Satellite Scatterometer Data." *ISPRS Journal of Photogrammetry and Remote Sensing* 64 (4): 367–380. doi:10.1016/j.isprsjprs.2009.01.004.
- Paget, A. C., S. Frolking, D. G. Long, and T. Milliman. 2014. *MERS Report 14-01: Observations of Spatial and Temporal Variations in σ^0 for QuikSCAT LIB in Urban Areas, Report*. Microwave Earth Remote Sensing, Provo, UT: Brigham Young University. <http://www.mers.byu.edu/docs/reports/MERS1401.pdf>
- Parera, C. 2005. "Mormon Town Planning: Physical and Social Relevance." *Journal of Planning History* 4 (2): 155–174. doi:10.1177/1538513205275437.
- Spencer, M. W., C. Wu, and D. G. Long. 2000. "Improved Resolution Backscatter Measurements with the SeaWinds Pencil-Beam Scatterometer." *IEEE Transactions on Geoscience and Remote Sensing* 38 (1): 89–104. doi:10.1109/36.823904.
- Steele-Dunne, S. C., J. Friesen, and N. van de Giesen. 2012. "Using Diurnal Variation in Backscatter to Detect Vegetation Water Stress." *IEEE Transactions on Geoscience and Remote Sensing* 50 (7): 2618–2629. doi:10.1109/TGRS.2012.2194156.
- Ulaby, F., and D. G. Long. 2014. *Microwave Radar and Radiometric Remote Sensing*. Ann Arbor: University of Michigan Press. ISBN 978-0472119356. http://www.press.umich.edu/7162328/microwave_radar_and_radiometric_remote_sensing
- Ulaby, F., R. Moore, and A. Fung. 1981. *Microwave Remote Sensing Active and Passive Vol. 1: Microwave Remote Sensing Fundamentals and Radiometry*. Reading, MA: Addison-Wesley, Advanced Book Program.
- Wu, C., Y. Liu, K. H. Kellogg, K. S. Pak, and R. L. Glenister. 2003. "Design and Calibration of the SeaWinds Scatterometer." *IEEE Transactions On Aerospace Electronic Systems* 39 (1): 94–109. doi:10.1109/TAES.2003.1188896.